Received 4 October 2019; revised 21 November 2019; accepted 25 November 2019. Date of publication 9 January 2020;
date of current version 27 April 2020. The review of this article was arranged by Editor L. F. Marsal.

Digital Object Identifier 10.1109/JEDS.2020.2965213

Origin of the Negative Differential Resistance in the Output Characteristics of a Picene-Based Thin-Film Transistor

ELOI ROS, JOAQUIM PUIGDOLLERS, PABLO ORTEGA, AND CRISTOBAL VOZ

Departament Enginyeria Electrònica, Universitat Politècnica Catalunya, 08034 Barcelona, Spain

CORRESPONDING AUTHOR: J. PUIGDOLLERS (e-mail: Joaquim.puigdollers@upc.edu)

This work was supported in part by the Spanish Government under Project ENE2016-78933-C4-1-R and Project ENE2017-87671-C3-2-R.

ABSTRACT In this work, we have fabricated and studied p-type picene thin-film transistors. Although the devices exhibited good electrical performance with high field-effect mobility (up to 1.3 $cm^2/V{\cdot}s$) and on/off ratios above 10^5, the output electric characteristics of the devices exhibited a Negative Differential Resistance for higher drain-source voltage. Finally, a possible explanation for this phenomenon is developed.

INDEX TERMS OTFT, NDR, organic semiconductors, non-ideal output.

I. INTRODUCTION

Thin-Film Transistors based on organic semiconductors (OTFT) is one of the key device in modern electronics. Organic compounds incorporate semiconducting materials often based on π-conjugated bonds that are mechanically compatible with flexible substrates, opening a new fan-out opportunity for emerging applications. Examples span from healthcare-monitoring devices [1], electronic newspapers [2], organic information storage devices [3], flexible displays [4], and flexible radio frequency identification tags [5].

However, almost all electronic devices used in daily life are based on inorganic semiconductors, such as silicon, gallium arsenide, indium phosphide, etc. Most of this inorganic Field Effect Transistors (FET) owned their place on the market due to their high operating speed, and environmentally stable everlasting performance. In order to make OTFT appealing to future industry, technical issues related to structures, materials, models, operating principles, fabrication and *device performance parameters* have to be solved [6].

An important issue that must be addressed is the deviation observed in OTFTs current-voltage output, from the expected transistor behaviour [7]. This non-ideal performance and lack of consistence in the transistor behaviour is probably related to physical phenomena and undesired interactions potentially leading to variability on the resulting *transistor parameters*.

One of the irregularities often observed in OTFTs is the presence of Negative Differential Resistance (NDR) in the saturation region of the output curve of the device, i.e., an increase in drain-source voltage (V_{DS}) results in a decrease in drain-source current (I_{DS}) for a fixed gate-source voltage (V_{GS}) [8], [9]. Understanding the origin of the NDR effect could provide guidelines for interpreting this particular non-ideality usually found in high mobility OTFTs, and give new design rules for the manufacturing of devices with higher reliability. Finally, we have fabricated OTFTs based on p-type picene semiconductor. Electrical characterization of the devices showed a marked NDR effect in the saturation region of the output $I_{DS}(V_{DS})$ curve. An explanation of the physical origin of the observed negative differential resistance is described by taking into account the effect of the V_{DS} on the gate voltage, and the geometry of the device. Finally, an analytical model is developed including some of the previously discussed premises obtaining a simple equation that accounts for NDR.

II. EXPERIMENTAL

We fabricated the OTFTs using the inverted-staggered (top contact) structure shown schematically in Figure 1. The substrate consisted of a thermally oxidized silicon wafer with a thickness of 120 nm for the SiO_2 dielectric.

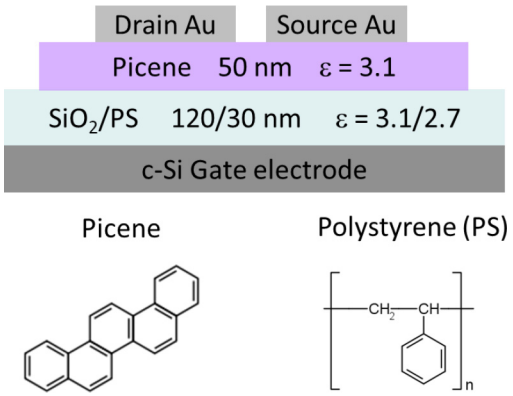

FIGURE 1. (Top) Scheme of the fabricated TFT based on picene. Thicknesses and permitivitty values of the picene and dielectric layer are showed. (Bottom) Chemical structure of the picene and polystyrene molecule.

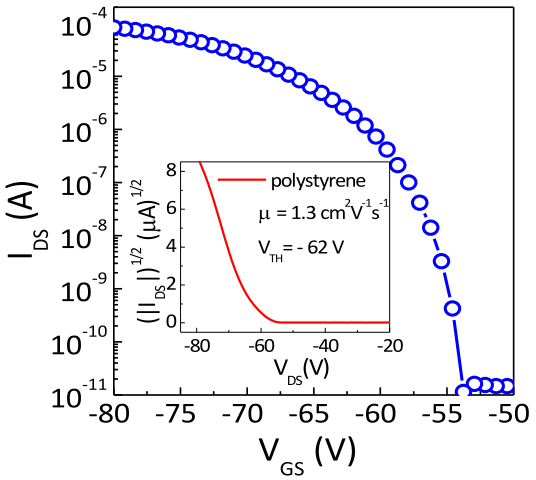

FIGURE 2. Transfer characteristics. (Inset) Saturation characteristcics, from which the field-effect mobility and Threshold voltage are estimated.

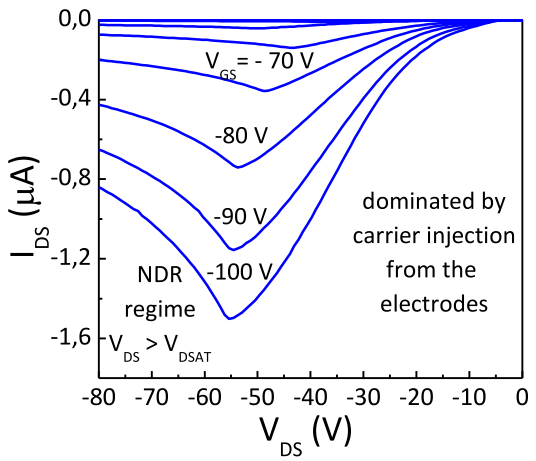

FIGURE 3. Output characteristics of the picene-based TFT. NDR effect is observed for V_{DS} voltages higher than V_{DSAT}.

A polystyrene (PS) layer of 30 nm was deposited by spin-coated on top of the SiO_2 dielectric layer in order to improve the crystallinity of the picene thin-film layer. Therefore, the capacity of the insulator (SiO_2/PS) per unit area was 20 nF·cm^{-2}. Picene and PS compounds, purchased from Sigma–Aldrich, were used without further purification. The active picene layer (50 nm) was deposited in a vacuum system with base pressure below 10^{-6} mbar and the sublimation temperature was regulated near to 135 °C to maintain a stable deposition rate around 0.5 Å/s. After picene deposition, the samples were transferred to a different vacuum chamber used to evaporate metallic contacts. The drain and source gold electrodes were defined by means of a metallic shadow mask, with a channel length (L) and width (W) of 50 μm and 600 μm, respectively. The fabricated OTFTs were electrically characterized in air and under vacuum conditions (10^{-1} mbar) using an Agilent 4156C parameter analyser.

The charge carrier mobility (μ) and the threshold voltage (V_{th}) were estimated in the saturated region by using the following equation:

$$I_D = \frac{WC_{ox}\mu}{2L}(V_{GS} - V_{th})^2 \quad (1)$$

where W and L are the channel width and length, respectively, and C_{ox} is the capacitance of the dielectric per unit area.

Figure 2 shows the transfer and the saturation characteristics of the device, showing an excellent p-type behaviour. From the saturation curve (inset of Figure 2) the carrier field-effect mobility and threshold voltage were estimated.

Plotted in Figure 3 one can observe the output current obtained from the picene TFT. When a low V_{DS} is applied, one can see that the current does not scales linearly with the applied voltage. This probably indicates a crowding effect near the contact as a result of a poor carrier injection at the electrodes. For higher V_{DS} values we would expect a saturation of the I_{DS} on a functional transistor. Instead, as seen in Figure 3 the current output starts to decrease as the voltage increases. This phenomenon is usually named as negative differential resistance (NDR) regime, and appears for V_{DS} voltages values higher than $V_{DS\text{-}SAT}$.

The origin of this NDR effect is yet unclear. A possible explanation could be argued based on the geometry of the transistor and the different values of the dielectric constants of the semiconductor and insulator. The variation of I_{DS} upon the application of V_{DS} is usually explained by the change of the accumulated charge at the semiconductor/dielectric interface induced by the application of V_{GS} (field-effect phenomenon). Consequently, the applied V_{GS} controls the *electrical resistance* of the channel and therefore the I_{DS} [10].

Nevertheless, one can understand the FET by analysing the relative energy level position of the different elements involved in the device. Therefore, the electrical output of a TFT can be understood from the position of the Fermi level of the drain, source and semiconductor [11]. First, when the device is in equilibrium, Fermi level must be equal everywhere. The external application of a V_{DS} will

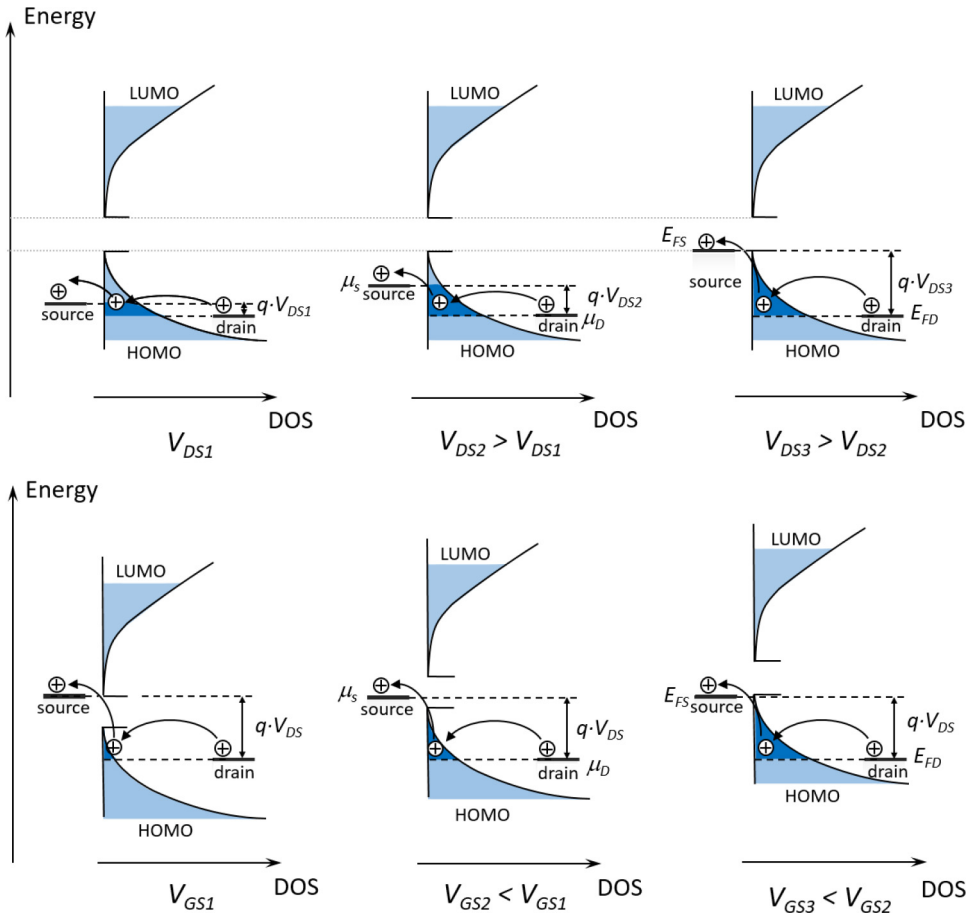

FIGURE 4. **(Top) Schematic representation of the energy levels of the source, drain and DOS of the p-type picene TFT for a changing V_{DS}. (Bottom) Schematic representation of the energy levels of the source, drain and DOS of the p-type picene TFT for a changing V_{GS}.**

split away the Fermi level of the drain and source electrodes ($E_{F1} - E_{F2} = -\mathrm{q} \cdot V_{DS}$).

In order to drive the system again into equilibrium, carriers (holes in our picene TFT) will flow between source and drain electrodes through available electronic states at the semiconductor. In this view the flow of carriers will be motivated by an external potential gradient that allows carriers on one electrode to reach a lower energetic state available on the other electrode, thus, filling the electronic states until Fermi level of the electrodes reach once again equilibrium conditions ($E_{F1} = E_{F2}$). In this picture, the external applied voltage (V_{DS}) maintains the electrodes Fermi levels separated, continuously pulling the system out of equilibrium, and eventually yielding a continuous carrier flow between both electrodes; as carriers keep trying to drive the system back into equilibrium forced by the external voltage applied onto the Drain.

However in order to obtain a true picture of the device one must include the available conducting energy states inside the semiconductor, as the device current (I_{DS}) or the carriers flow will be limited by the amount of available states (Density-of-States (DOS)) in the semiconductor, between the energy window defined between the Fermi levels of the electrodes, i.e., $E_{F1} - E_{F2}$.

In the particular case of a p-type semiconductor, like picene, these electronic states will be located around the HOMO level of semiconductor (HOMO corresponds to the High Occupied Molecular Orbital of the semiconductor). One can see in Figure 4 (top) a schematic representation of the energy levels of the source and drain electrodes and the difference obtained in terms of the location of the Fermi level upon the application of negative V_{DS} (applied to the drain with respect to the source).

The window of available conduction states of the semiconductor between source and drain Fermi levels has been coloured on the schematic DOS of the semiconductor. It looks intuitive from this picture that a higher applied V_{DS} results in a larger I_{DS}. The saturation of the output in this model is understood from the limited amount of available states in the semiconductor. This means that when V_{DS} is larger than $V_{DS\text{-}SAT}$ there are no more available conducting states in the semiconductor and the rate of carriers that flow through the semiconductor will remain equal, regardless of an increase in external voltage.

Let us examine the situation when a voltage is applied to the gate with respect to the source (Figure 4 (down)). In this case the negative V_{GS} changes the potential in the semiconductor channel displacing its Fermi level upwards.

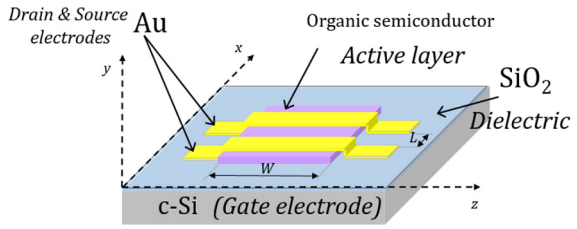

FIGURE 5. Geometric description of the model of the transistor.

The displacement of the Fermi level of the semiconductor will pull all electronic states up in energy. Therefore, an increase in V_{GS} triggers an increase of DOS between the Fermi levels of the electrodes.

Since Fermi levels of the source and drain remains unaffected (V_{DS} has not changed) the increase of DOS between $E_{F1} - E_{F2}$ yields an increase in I_{DS}, as shown in Figure 4 (down).

In conclusion, increasing V_{GS} results in more electronic states available in the channel for conduction, and therefore an increase of the Drain Source current.

Furthermore, the existence of a threshold gate voltage (V_{th}) as the voltage needed to turn the transistor *on* can be explained by the energy difference between the equilibrium Fermi level of the semiconductor ($E_{SC} = E_{F1} = E_{F2}$) and the lowest available empty electronic state of the semiconductor, that in the case of p-type semiconductor corresponds to the HOMO conduction edge.

Finally, since from this model one can describe the working principle of a TFT, we believe that this model can be used to provide an explanation of the NDR effect that appears at higher V_{DS} voltages on the output characteristic of our picene devices.

It is important to point out that our TFT structure is quite symmetrical from the point of view of the active and dielectric layer. This means that the thicknesses of the picene and the dielectric layers lie on the same order of magnitude. Furthermore, dielectric constants of the picene and the SiO2/PS layers have similar values. Therefore, the application of a V_{DS} splits the Fermi levels of the source and drain electrodes apart, as previously commented, but because of the geometric location of the electrodes and the channel as well as the existing symmetry between dielectric and semiconductor layer, the voltage applied also affects the position of the DOS of the semiconductor. Which in this case it would affect it by displacing it in the opposed direction of V_{GS}. This effect is more prominent in the saturation region, when the channel pinch-off has already happened.

III. MODELING NDR

A derivation of the NDR behavior characteristic of the picene top contacts thin film transistors can be analytically derived from the geometry seen in Figure 5 by introduction of a NDR parameter (i.e., r_{NDR}) intrinsic to each organic semiconductor one may use.

One can assume that the main current output will be given by the conduction of the charge accumulated in the channel, a common assumption in MOSFET devices [12]. For the most part this current in the channel can be written as the product of a drift [13].

$$\begin{aligned} I &= \int_y \int_z J_x dz dy = \int_0^W \int_0^{t_{sc}} \sigma E_x dz dy \\ &= \int_0^W \int_0^{t_{sc}} e\mu_p p(y) E_x dz dy \\ &= \mathrm{W} e\mu_p E_x \int_0^{t_{sc}} p(y) dy = \mathrm{W}\mu_p \frac{dV_{ch}}{dx} \int_0^{t_{sc}} ep(y) dy \\ &= \mathrm{W}\mu_p \frac{dV_{ch}}{dx} Q_p \end{aligned} \tag{2}$$

In this picture $\mathrm{V_{ch}}$ is the voltage at each point of the channel, μ_p is the hole mobility and Q_p is the hole charge accumulated in the channel at the semiconductor/dielectric interface. This charge is shown to be proportional to the applied gate voltage following equation (3) [14]:

$$Q_p = C_{ox}[(V_{GS} - V_{ch}(x) - V_T)] \tag{3}$$

Now with the complete picture of the amount of charge present in the channel we can proceed to calculate the output intensity by means of a spatial integration of (2).

$$\begin{aligned} \int_0^L I dx &= \mathrm{W}\mu_p \int_0^L \frac{dV_{ch}}{dx} Q_p dx \\ &= W\mu_p C_{ox} \int_0^L \frac{dV_{ch}}{dx} (V_{GS} - V_x - V_T) dx \end{aligned} \tag{4}$$

The integral becomes independent of x, and can be finally written as:

$$I = \frac{W}{L} \mu_p C_{ox} \int_{\mathrm{V_{ch}}(0)}^{V_{ch}(L)} (V_{GS} - V_{ch} - V_T)\ dV_{ch} \tag{5}$$

With this expression the classical output of a MOSFET is obtained when we define an equipotential contact between the channel and the electrode (i.e., $\mathrm{V_{ch}}(0) = V_S$ and $\mathrm{V_{ch}}(L) = V_D$). However, as previously discussed the geometry of the fabricated device allows us to assume that there are other effects constraining this assumption.

For instance, due to the position of the electrodes across the organic semiconductor layer a decrease in voltage in the channel with respect to the external applied V_{DS} is possible due to multiple effects.

The aforementioned voltage difference due to V_{GS}/V_{DS} interaction can be simplified as a factor proportional to the current flow in the channel as shown in Figure 6 (i.e., $\mathrm{V_{ch}}(0) = V_S - r_{NDR} \cdot I$ and $\mathrm{V_{ch}}(L) = V_D - r_{NDR} \cdot I$) as the intensity of the drift current is a measure the amount of charge present due to the MOS capacitor.

With this assumption one can perform a modified version of the classical integral using $\Delta V = r_{NDR} I$:

$$I = \frac{W}{L} \mu_p C_{ox} \int_{V_S + \Delta V}^{V_D - \Delta V} (V_{GS} - V_{ch} - V_T)\ dV_{ch} \tag{6}$$

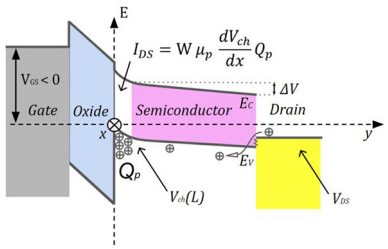

FIGURE 6. Band schematic of the MOS capacitor for a non-zero drain-source voltage including a voltage difference between drain and gate electrodes.

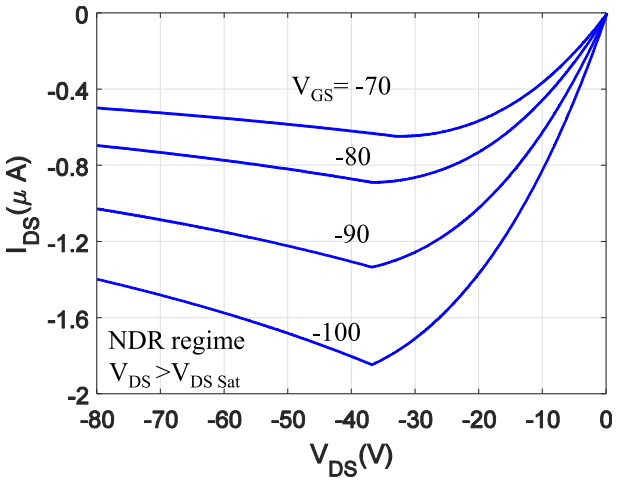

FIGURE 7. Drain Source current plot as a function of V_{DS} obtained out of Eq. (8) using the parameters extracted from the picene transistors.

$$LI = W\mu_p C_{ox}\left[(V_{GS} - V_T)V_{DS} - V_{DS}^2/2\right] - W\mu_p C_{ox} r_{NDR} I(2(V_{GS} - V_T) - V_{DS}) \quad (7)$$

Which finally yields the expression:

$$I_D = \frac{\frac{W}{L}\mu_p C_{ox}\left[(V_{GS} - V_T)V_{DS} - \frac{V_{DS}^2}{2}\right]}{1 + \frac{W}{L}\mu_p C_{ox} r_{NDR}[V_{DS} - 2(V_{GS} - V_T)]} \quad (8)$$

Using the parameters extracted from the fabricated picene OFETs and a value of $r_{NDR} = 2 \cdot 10^4 \Omega$, one can see as plotted in Figure 7 how the equation obtained reproduce a Negative Differential Resistance similar to the observed in the device. The clearest difference is seen at low V_{DS} where current crowding at the contact is not observed as in the case of the fabricated picene devices. Nevertheless, the inflexion point that related to the beginning of the NDR regime is also reproduced by the equation, as for $V_{DS} > V_{DS\text{-}Sat}$ the DOS available in the channel saturates and therefore numerator of the equation remains constant while the interaction between V_{DS} and V_{GS} is still actively modifying the total current of the device.

$$I_D = \frac{\frac{W}{L}\mu_p C_{ox}\left[\frac{(V_{GS} - V_T)}{2} V_{DS\ Sat}^2\right]}{1 + \frac{W}{L}\mu_p C_{ox} r_{NDR}[V_{DS} - 2(V_{GS} - V_T)]} \quad (9)$$

In conclusion, the increasing amount of voltage difference (i.e., $V_c(0) - V_S$ and $V_c(L) - V_D$) between the contacts and the channel represented in the equations by this r_{NDR} factor, is affecting the output of the transistor by means of an increasingly sharpened NDR effect for a larger V_{GS} values.

IV. CONCLUSION

The existence of Negative Differential Resistance measured in picene-based thin-film transistors can be explained by taking into account the geometry of the device and the permittivity of both, active and dielectric layer. The application of a large drain-source voltage counteracts the charge accumulation effect generated by the gate-source voltage near the drain contact (i.e., it displaces the DOS of the semiconductor in the opposite direction of an external V_{GS}), thereby *reducing* the number of available states in the channel and progressively decreasing the I_{DS} current.

REFERENCES

[1] Y. Zang, F. Zhang, D. Huang, X. Gao, C.-A. Di, and D. Zhu, "Flexible suspended gate organic thin-film transistors for ultra-sensitive pressure detection," *Nat. Commun.*, vol. 6, p. 6269, Mar. 2015, doi: 10.1038/ncomms7269.

[2] F. Eder, H. Klauk, M. Halik, U. Zschieschang, G. Schmid, and C. Dehm, "Organic electronics on paper," *Appl. Phys. Lett.*, vol. 84, no. 14, p. 2673, 2004, doi: 10.1063/1.1690870.

[3] Z. Bao, A. J. Lovinger, and A. Dodabalapur, "Organic field-effect transistor with high mobility based on copper phtalocyanine," *J. Appl. Phys. Lett.*, vol. 69, no. 20, p. 3066, 1996, doi: 10.1063/1.116841.

[4] G. H. Gelinck, E. A. Huitema, E. Van Veenedaal, E. Cantatore, P. Tom, and C. T. Giesbers,

[5] G. H. Gelinck *et al.*, "Flexible active-matrix displays and shift registers based on solution-processed organic transistors," *J. Nat. Mater.*, vol. 3, pp. 106–110, Jan. 2004, doi: 10.1038/nmat1061.

[6] V. Fiore *et al.*, "An integrated 13.56-MHz RFID tag in a printed organic complementary TFT technology on flexible substrate," *IEEE Trans. Circuits Syst. I, Reg. Papers* vol. 62, no. 6, pp. 1668–1677, Jun. 2015, doi: 10.1109/TCSI.2015.2415175.

[7] B. K. Kaushik, B. Kumar, Y. S. Negi, and P. Mittal, "Prospects and limitations of organic thin film transistors (OTFTs)" in *Advances in Computer Science, Engineering & Applications*, vol. 167. Berlin, Germany: Springer.

[8] H. Gomes, *Organic Field-Effect Transistors*. 2016, doi: 10.4032/9789814669757.

[9] J. S. Jung, E. H. Cho, S. Jo, K. H. Kim, D. H. Choi, and J. Joo. "Photo-induced negative differential resistance of organic thin film transistors using anthracene derivatives," *Org. Electron.*, vol. 14, no. 9, pp. 2204–2209, 2013, doi: 10.1016/j.orgel.2013.05.019.

[10] K. H. Lee and S. Cristoloveanu, "Esaki diode in undoped silicon film," *IEEE Electron Device Lett.*, vol. 40, no. 9, pp. 1346–1349, Sep. 2019.

[11] S. Gomes, *Organic and Printed Electronics—Fundamentals and Applications*, G. Nisato, D. Lupo, and S. Ganz, Eds. Boca Raton, FL, USA: CRC Press, 2016, Ch. 5.

[12] S. Datta, "Electronic transport in mesoscopic systems," in *Cambridge Studies in Semiconductor Physics and Microelectronic Engineering*. Cambridge, U.K.: Cambridge Univ. Press, 1997.

[13] S. M. Sze, *Physics of Semiconductor Devices*. Hoboken, NJ, USA: Wiley, 2007.

[14] K. F. Brennan, *The Physics of Semiconductors With Applications to Optoelectronic Devices*. Cambridge, U.K.: Cambridge Univ. Press, 1999.

[15] S. Wang, *Fundamentals of Semiconductor Theory and Device Physics*. Englewood Cliffs, NJ, USA: Prentice-Hall, 1989.